Journal of Catalysis 270 (2010) 275–284

Contents lists available at ScienceDirect

Journal of Catalysis

journal homepage: www.elsevier.com/locate/jcat

Multitechnique analysis of supported Pd particles upon dynamic, cycling CO/NO conditions: Size-dependence of the structure–activity relationship

Anna Kubacka [a], Arturo Martínez-Arias [a], Marcos Fernández-García [a,*], Marco Di Michiel [b], Mark A. Newton [b,*]

[a] Instituto de Catálisis y Petroleoquímica, CSIC, C/Marie Curie 2, 28049 Madrid, Spain
[b] European Synchrotron Radiation Facility, 6, Rue Jules Horowitz, BP-220 Grenoble, France

ARTICLE INFO

Article history:
Received 28 October 2009
Revised 31 December 2009
Accepted 6 January 2010

Keywords:
Pd three-way catalysts
Alumina
In situ-DRIFTS
XAS
HXRD
MS

ABSTRACT

The behaviour of Pd/Al_2O_3 supported catalysts with metal loading in the 0.5–4 wt.% interval has been examined during cycling CO/NO conditions in an attempt to interpret the size-dependence of the metal chemical activity within a dynamic redox situation. To this end, a synchronous, multitechnique approach using X-ray absorption (XAS) or hard X-ray diffraction (HXRD) in tandem with diffuse reflectance infrared spectroscopy (DRIFTS) and mass spectrometry (MS) was used to establish the size-dependence of chemically significant steps in formation of N_2 and CO_2. During cycling, EXAFS and HXRD reveal the existence of a reversible Pd morphology and phase change (PdC_x formation and removal) phenomena in response to the gas atmosphere reducing/oxidizing nature. This is observed for Pd particles having dispersion values going from ca. 1–0.4. Using EXAFS Pd–Pd coordination numbers, we dynamically normalized the DRIFTS and MS signals obtained during cycling conditions and find that metal size/phase-effects appear of importance in CO_2 formation but can be essentially neglected in N_2 formation. Such (size-dependent) metal behaviour appears far from expectations coming from studies using non-cycling gas mixtures. The chemical relevance of NO, CO activation, dissociation and coupling steps are discussed in relation to the product formation and their size-dependence or independence.

1. Introduction

Noble metals are key components in a number of critical technological areas related to catalysis [1]. Among catalytic processes, automobile catalysts and, particularly, three-way catalysts (TWCs) appear as a representative example illustrating scientific and technological innovation and giving novel perspectives for chemistry and material sciences [2–4]. TWCs have been widely used to diminish polluting emissions from gasoline engine powered vehicles. Current systems contain Pd as the main component though the drivers for this being the case are principally economic (Pd is currently cheaper than Rh). However, the remarkable intrinsic activity of Pd for oxidation reactions concerning carbon monoxide and hydrocarbons, and its reasonably good resistance to sulphur poisoning in standard conditions, e.g. with current low-sulphur (20 ppm) fuels, are also highly significant scientific factors that make this current trend realizable.

Pd-based TWCs have been extensively studied under light-off or isothermal conditions but much less is known for cycling conditions, typical of TWC operation. In these cases the stoichiometry of the gas atmosphere oscillates around the stoichiometric point with a frequency of ca. 1–3 Hz [2–4]. Under such dynamic conditions, both the metal [5–7] and the metal-promoter interface [5,8–11] behaviours are of critical importance. In this contribution, using Pd/Al_2O_3 systems as models, we focus on the role of nanoparticle size on the structural–temporal response of the supported nanoparticles, and the interrelated consequences these might have for chemical activity. $Pd–Al_2O_3$ contacts are of importance in TWC systems as they are critical in promoting NO reduction reactions [8,12–14]. As such, as a system where metal particle size can be reasonably well isolated from metal–support interaction, as well as for the practical reasons related to NO reduction, $Pd–Al_2O_3$ appears as the correct system to analyse the influence of Pd size in cycling CO/NO conditions. In Pd model systems, while the CO oxidation ($CO + O_2$) reaction is essentially considered surface and size insensitive [15], the CO + NO reaction turns out to be structure sensitive [16]. A weak sensitivity to the structure can nevertheless be observed for small Pd particles in the first reaction, as CO desorption (the limiting step in stoichiometric conditions) has a slight dependence on particle size [17]. Additional effects in this respect relate to the size dependence of the metal oxidation by oxygen-containing molecules [18,19], and, as detailed below, of CO dissociation [20].

The second reaction appears structure sensitive since NO dissociation and, in particular, N recombination to give N_2 are likely

* Corresponding authors. Fax: +34 91 585 4760.
E-mail addresses: m.fernandez@icp.csic.es, mfg@icp.csic.es (M. Fernández-García), newton@esrf.fr (M.A. Newton).

0021-9517/$ - see front matter © 2010 Elsevier Inc. All rights reserved.
doi:10.1016/j.jcat.2010.01.008

favoured for small and large Pd particles, respectively [12,15,21,22]. As such, analysis of CO and NO adsorption and metal surface interactions, as well as their respective dissociation and fragment recombination – to give N_2/CO_2 – as a function of the Pd particle size is of significant importance to rationalize the behaviour of TWCs as well as to understand these basic reaction steps in many other chemical processes.

As with many functional materials, the Pd/Al_2O_3 system shows structural variation on a wide range of length scales going from the chemical bond, through nanosize component phase, and, eventually, to the micron scale. This provides a strong driving force to multitechnique approaches able to address all physico-chemical phenomena taking place in the system under "operando" (e.g. reaction) conditions [5,23–27].

Very useful in catalysis are those methodologies which combine surface and bulk sensitive techniques and, particularly, those capable of having a sufficient time resolution to discriminate the multitude of structural and electronic phenomena occurring upon contact and reaction with gas mixtures. Here we make a subsecond time resolved study of Pd/Al_2O_3 catalysts during CO/NO cycling conditions using two structural techniques X-ray absorption structure (XAS) and X-ray diffraction (XRD). The same sample environment and conditions are used to collect the EXAFS and XRD data and, in each case, these measurements are conjoined with parallel analysis of the gas–solid interface using time resolved infrared spectroscopy (diffuse reflectance infrared spectroscopy, DRIFTS) and global activity/selectivity using mass spectrometry (MS). By correlating the structural (XRD/EXAFS), surface (DRIFTS) and gas phase (MS) information available using this approach we aim to illustrate how key elemental steps (e.g. adsorption, dissociation, surface recombination, and desorption of products) manifest themselves as a function of Pd particle size. From this we may then further understand their interplay and which, if any, appear key in determining chemical activity. Our findings illustrate how important is to have access to time-dependent structural information to correctly describe the size dependence or independence of the physical phenomena occurring in Pd upon cycling conditions.

2. Experimental methods

Four Pd/Al_2O_3 samples were synthesized by a wet impregnation method using a palladium nitrate solution (10 w/w%) and gamma alumina (Condea Puralox; S_{BET} 180 $m^2\,g^{-1}$) [28]. Pd loadings were 0.5, 1, 2 and 4 wt.% (metal basis) and corresponding samples are named, respectively, as *x*PdA, where *x* is the wt.% of the noble metal. After calcination at 773 K for 2 h, catalysts display the same surface area values (within error) as the bare support. TEM analysis of the samples was carried out with a JEOL 2010FX instrument. Samples were dispersed in iso-propanol on lacy carbon support films.

The experimental set-up allows working with one structural technique (XAS or XRD) synchronously with DRIFTS and MS techniques [6,7,29]. In all experiments, ca. 30–40 mg of sample, sieved to a 80–100 μm fraction, were used. Experiments were carried out on beamlines ID15B (XRD) and ID24 (Dispersive-XAS) at the European Synchrotron Radiation Facility (ESRF). Diffraction measurements were collected at 86.8 keV with a digital flat 2D panel (Pixium 4700) detector at 1300 mm from the sample position. Absorption experiments at the Pd K-edge utilized a Si(3 1 1) polychromator in Bragg configuration and a 16bit CCD FreLoN detector [30]. DRIFTS measurements were made using a Bruker IFS 66 spectrometer coupled with a MCT detector. Gas flows were controlled by Bronkhorst mass flow controllers. Samples were heated under a flow of He to 673 K and then subjected to cycling comprising alternative (CO first) flows (75 ml min^{-1}; corresponding to a "stationary" GHSV ca. 80,000 h) of 5% CO/He (13.84 s) and 5% NO/He (13.84 s) while XAS/XRD, DRIFTS and MS data were collected synchronously.

EXAFS analysis was carried out using standard procedures, and Pd–Pd coordination numbers (C.N.s) were obtained using a fixed Debye–Waller (DW) factor [6]. The value of the DW factor used is determined via equating the Pd–Pd C.N. derived post-reaction at room temperature (RT) under He with that derived post-reaction at 673 K under He. Axiomatic to this approach is the assumption that the DW static contribution does not change upon cooling from 673 K to RT under He. Once the Pd–Pd C.N. is obtained, the dispersion (expressed as the number of surface atoms vs. the total number of atoms) is calculated via the Jentys procedure which allows to obtain the number of atoms associated with a Pd–Pd C.N. [31]. Dispersion values assume cubo-octahedral shapes for the Pd particles [23] and are subsequently used to normalize DRIFTS and MS signal intensities with the help of a smoothing spline interpolation program [32].

3. Results

The apparent behaviour, within the overall paradigms of the analysis applied, of the Pd–Pd C.N. upon the CO/NO cycling conditions is presented for 1PdA, 2PdA and 4PdA in Fig. S1 (Supporting Information). Sample 05PdAl is not presented as the small particle size does not allow an EXAFS analysis at reaction conditions (673 K). According to XANES (result not shown) and as discussed previously [6,7], all samples are in a fully metallic state at pseudo-stationary conditions, e.g. after the 3rd cycle. Fig. 1 shows a representative CO/NO cycle (average of two experiments; Fig. S1 shows a typical full experiment), allowing to observe fine details of the reversible morphological changes suffered by the metal particles at such conditions. During CO exposure and after an initial stationary period, the C.N. goes up and maintains a high value up to the first seconds of the next NO step to subsequently recover the initial situation. In the high coordination number region, which takes place at the final/initial parts of the CO/NO steps, all samples behave similarly although the valley structure displayed by the Pd–Pd C.N. is more marked in the 1PdA sample. This is discussed below in the context of the multitechnique approach, but here we anticipate that such valley has been shown to be related to the formation and destruction of a PdC_x phase [33].

The Pd–Pd C.N. obtained from the EXAFS analysis is used in combination with Jentys analysis [31] in order to measure the dynamic behaviour of the metal dispersion under reaction conditions. Fig. 1B displays the metal dispersion of the above-mentioned samples. This parameter mirrors the behaviour of the C.N.s but with some differences in the valley region between maximum values. In that region, no change in particle size is assumed (see below). Dispersion values decrease from 1PdA to 2PdA and more acutely for 4PdA. The dispersion values and average particle size correspond well with the TEM distribution presented in Fig. 2 for the initial, oxidized state. TEM yields average particle sizes as ca. 2.2, 2.9 and 3.8 nm respectively for the 1, 2 and 4PdA systems. Relative morphology changes upon CO and NO (e.g. relative ratio between maximum and minimum values in Table 1) are roughly similar for all samples and display a moderate growth with metal loading. So, morphological changes are relatively more important in the particles with larger particle size. This is further discussed below.

We further note that in TEM analysis both the 1PdA and the 2PdA samples appear metallic. That is to say that lattice fringe spacing is observed to be 2.24 and 2.27 Å, respectively. However, the fringe spacings measured for the 4PdA system are indicative of PdO i.e. 2.6–2.65 Å. Both EXAFS and HXRD measurements made on the as prepared and used catalysts both show that at all Pd load-

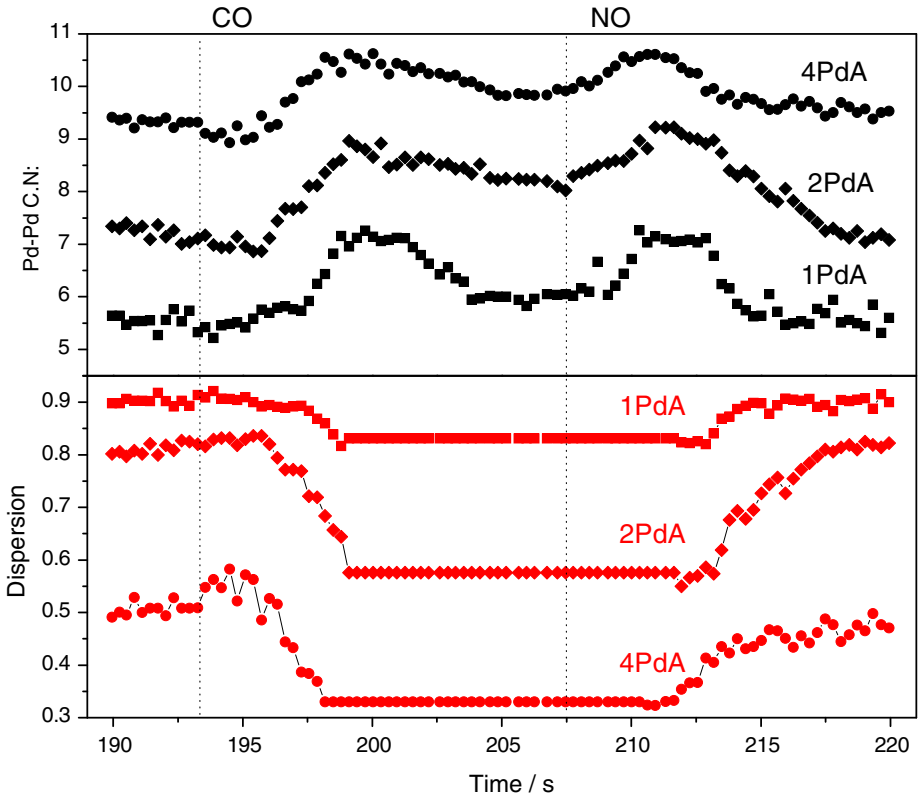

Fig. 1. EXAFS analysis of Pd–Pd 1st shell coordination number and metal dispersion over a CO/NO (5% in He; 75 ml min^{-1}) cycling treatment at 673 K. Samples are described as *x*PdA, where *x* is the noble metal weight loading percentage.

Table 1
Dispersion and relative total metal surface area of the *x*PdA samples.[a]

	1PdA	2PdA	4PdA
Dispersion			
Minimum	0.83	0.57	0.34
Maximum	0.95	0.82	0.53
Metal surface area			
Minimum	1	1.4	1.7
Maximum	1.15	2.0	2.55

[a] Standard errors; dispersion ±0.04; metal surface area ±0.05.

ings investigated the native form of the Pd these materials is nanoparticulate PdO. As such we conclude that in the 1PdA and 2PdA samples, the TEM measurements themselves have elicited the reduction in the PdO whereas at the 4 wt.% level the PdO resists modification in this manner. From the point of view of making truly valid comparisons between these systems and between techniques, this means that the normalized particle size distributions (PSD) derived from the 4 wt.% sample need to be adjusted to account for the difference in molar volumes of Pd metal and PdO. Doing this now means that the model Pd diameter for the 4PdA system is reduced below 3.5 nm.

XRD data (Fig. 3) give a complementary view of the dynamic behaviour of the Pd during cycling. The Pd peaks show an obvious repetitive cyclic behaviour similarly to the XAS measurements (Fig. 1). However, in this case the change that is most obvious in the XRD is a reversible change in the d spacing in the reflections arising from the Pd nanoparticles. No corresponding changes are observed in the features due to the Al_2O_3. Specifically, this behaviour starts again from an initial "static" period upon introduction of CO and increases in an essentially linear manner up to the end of the CO step. The switch back to NO leads to a rapid reversal of this effect resulting in the observed "sawtooth" type behaviour. Well-defined peak variations are observed. This can be clearly observed in Fig. 4 for the Pd(1 1 1) and Pd(3 1 1) reflections (located at *q* values ca. 2.8 and 5.3 Å, respectively) while the same phenomenology is less evident, due to alumina peak overlapping and/or limited intensity, for Pd(2 0 0), Pd(2 2 0) and Pd(2 2 2) reflections (located at *q* values ca. 3.2, 4.5, and 5.6 Å, respectively). The corresponding structural variation in the palladium cell parameter is associated with the formation of a PdC_x phase within the CO phase of the experiment. The formation of this phase introduces atomic carbon at interstitial positions of the metal fcc structure [33]. C atoms are obtained as products of the "Boudouard" reaction ($2CO_a \rightarrow CO_{2g} + C_a$) occurring within a high coverage CO ad-layer.

Fig. 4 shows the Pd(1 1 1) and Pd(3 1 1) reflections behaviour during a representative CO/NO cycle for the 4PdA samples. The increasing PdPd distances agree with the formation of a PdC_x phase [34,35]. PdA samples display a similar behaviour than that reported in Fig. 4 but the maximum carbon content is $x = 0.065$, 0.095, and 0.08 for, respectively, 1PdA, 2PdA, and 4PdA [36]. This reveals a modest dependence with the Pd loading, displaying a maximum for the 2PdA sample. The latter can be related with the presence of a maximum in the number of under-coordinated surface sites allowing easy formation (essentially unactivated reaction step) of sub-surface carbide species [37].

The DRIFTS measurements of the samples are plotted in Fig. S2. Fig. 5 provides results for 1PdA as a representative example. Bare alumina (Fig. S2) only shows presence of NO(gas) at 1910/1835 cm^{-1} and NCO species at 2235 cm^{-1} [8,12–14]. The presence of Pd induces drastic differences in chemical activity and surface ad-species. Under CO (Figs. S2 and 5) we initially observed the presence of threefold/bridge coordinated NO (1770–780 cm^{-1}) as the major species at the metal particle surfaces, together with a

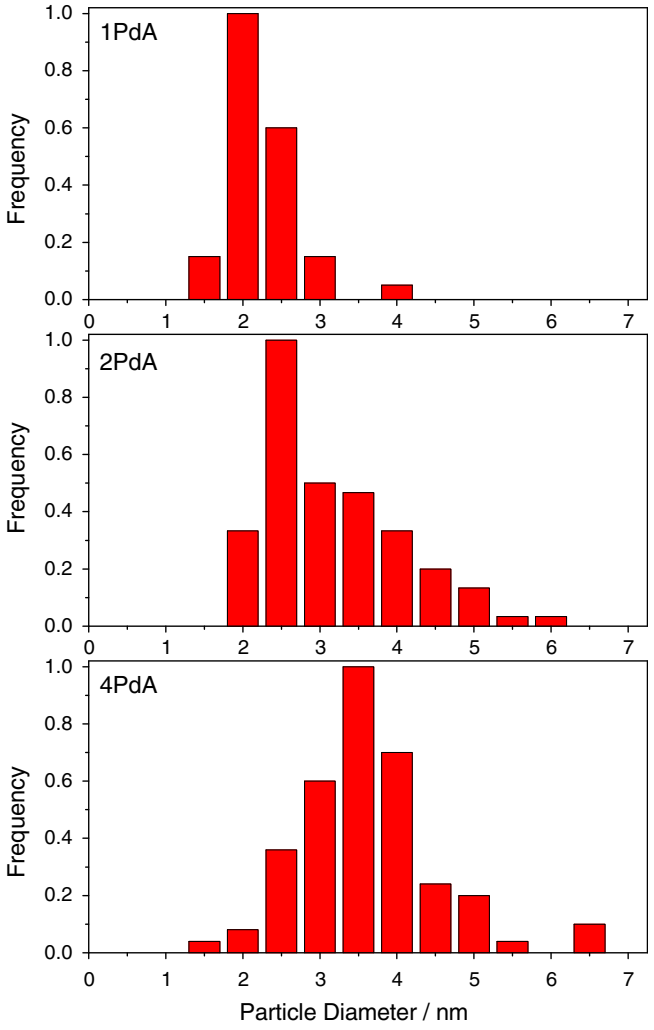

Fig. 2. Normalized particle size distributions (PSD) derived from TEM for calcined 1, 2, and 4 wt.% Pd on alumina catalysts.

small contribution of on-top species at ca. 1930 cm^{-1} for some samples (05PdA, 1PdA) [8,12,16,38–40]. The latter may overlap with a CO gas contribution. After ca. 2–3 s, CO ad-species form at the metal surfaces of all *x*PdA samples concomitantly to NO disappearance. Bridge-bonded species (1905–1940 cm^{-1}) are observed for all samples after NO disappearance from the surface with a typical shape dominated by dipolar coupling [41]. The atop sites (CO ad-species at 2040–2060 cm^{-1}) are also populated and, as shown in Fig. S2, all samples display roughly similar bridge to atop intensity ratios [8,13–16,19,22,38,39,42,43]. Fine details of the atop to bridge ratio can be, however, connected with the evolution of the PdC_x phase [33]. Such fine details are nevertheless not relevant for the present discussion. Besides CO and NO species adsorbed on Pd surfaces, the IR plots also provide evidence of formation of NCO absorbed on alumina sites and CO_2 gas (ca. 2356 cm^{-1}), as detected in the case of the bare support.

When switching from NO to CO, NCO is formed through the well-known $CO + N_a \rightarrow NCO$ reaction [8,16,39,40,42]. During the reverse switch (CO–NO) presented in Fig. 5, an unusual and rapid $NO + PdC_x \rightarrow NCO + Pd$ pathway is indicated alongside a more transitional $CO + NO \rightarrow NCO + O_a$ mechanism (see Section 4). We note that NO MS intensity does not fully recover up to the end of the NCO formation. In Figs. S2 and 5 there are also hints related to formation of carbonates species (region below 1600 cm^{-1}) but their roughly constant temporal behaviour for all samples is consistent with the being largely spectator species. This in itself is consistent with the well-established and limited contributions to chemical processes forming N_2/CO_2 and allows us to dismiss them as active protagonists in a first approximation [12].

The intensity plots for surface-adsorbed species vs. time are presented in Fig. 6. Raw and normalized (by metal dispersion extracted from Fig. 1B) data are displayed for all samples where XAS data analysis was possible. NCO is a difference signal where the contribution from bare Al_2O_3 is subtracted in order to allow a meaningful normalization. CO intensity correspond to the bridge species which is the most easily integrated; as the linear and bridge behaviour is roughly similar in all samples, and their ratio varies rather smoothly, the bridge species intensity behaviour is representative of all CO adsorbed species in respect to their contribution to CO_2 production. Besides that, the higher intensity and lower absorption coefficient of the bridge species clearly indicates that this corresponds to the dominant carbonyl species [44]. Raw NCO and CO intensities display a similar behaviour under CO atmosphere with a progressive intensity enhancement as a function of the Pd loading. Upon a NO atmosphere, NCO presents an abrupt increase with a maximum about ca. 2–3 s after the initial contact. The end of the NCO and CO ad-species signals occurs simultaneously. Adsorbed NO species display opposite behaviour to CO ones. As expected, they are present at the initial part of the CO cycling step but disappear after around 3 s without significant differences between samples. Upon NO atmosphere the intensity recovery of such ad-species is roughly similar for all samples although larger particles (2PdA and 4PdA samples) seem to cover the available metal surface with a slower rate. This produces a slower recovery of the NO intensity upon the NO atmosphere.

Important to note is that normalized signals in Fig. 6 display a behaviour with significant differences with respect to raw intensity. As a representative example, the number of NCO species per surface Pd atom: (i) decreases as a function of the Pd loading upon CO (e.g. 1PdA > 2PdA > 4PdA) while (ii) a roughly constant behaviour is observed upon a NO atmosphere. Normalized CO ad-species show less marked differences that those present in raw data although the trend as a function of particle size appears similar ($1PdA < 2Pd \leqslant 4PdA$) in both cases. Finally, some limited differences are observed for NO. The NO coverage per surface Pd atom appears roughly constant. However, upon introduction of CO there is a trend for lower stability of such ad-species as the Pd particle size decreases; that is, the NO species intensity decreases more quickly for 1PdA. This may indicate a lower binding interaction as the Pd particle size decreases.

As a final technique, we plot in Fig. 7 the MS results concerning selected signals labelled as (A) *M*/*z* 28, 30 and (B) 44. The first one contains major contribution from CO and N_2 molecules while 30 and 44 are, within present experimental conditions, mostly ascribed to NO and CO_2, respectively. Absence of significant quantities of N_2O at the analysed temperature is confirmed with the *M*/*z* 22 signal. Consumption of NO and CO is mostly apparent in the lower panel of Fig. 7 while reaction products are presented in the upper (CO_2) and lower panel (N_2 formation is detected as an "excess" signal over the decay trend of the *M*/*z* 28 signal). Trends in consumption and production of gas molecules as a function of the Pd content of the sample are better visualized in the difference plots (Al_2O_3 subtracted) displayed in Fig. 8. Similarly to the IR case, we show the difference raw (Fig. 8A) and per Pd surface atom normalized (Fig. 8B) data. For *M*/*z* 28 signal, difference plots allow an easy differentiation between NO consumption and N_2 formation as, respectively, negative and positive signals above the horizontal line of the upper panel of Fig. 8. In remaining panels, negative values correspond to gas-phase consumption reactions while positive ones describe the evolution of reaction products. Raw data show increasing CO and NO consumption in the order

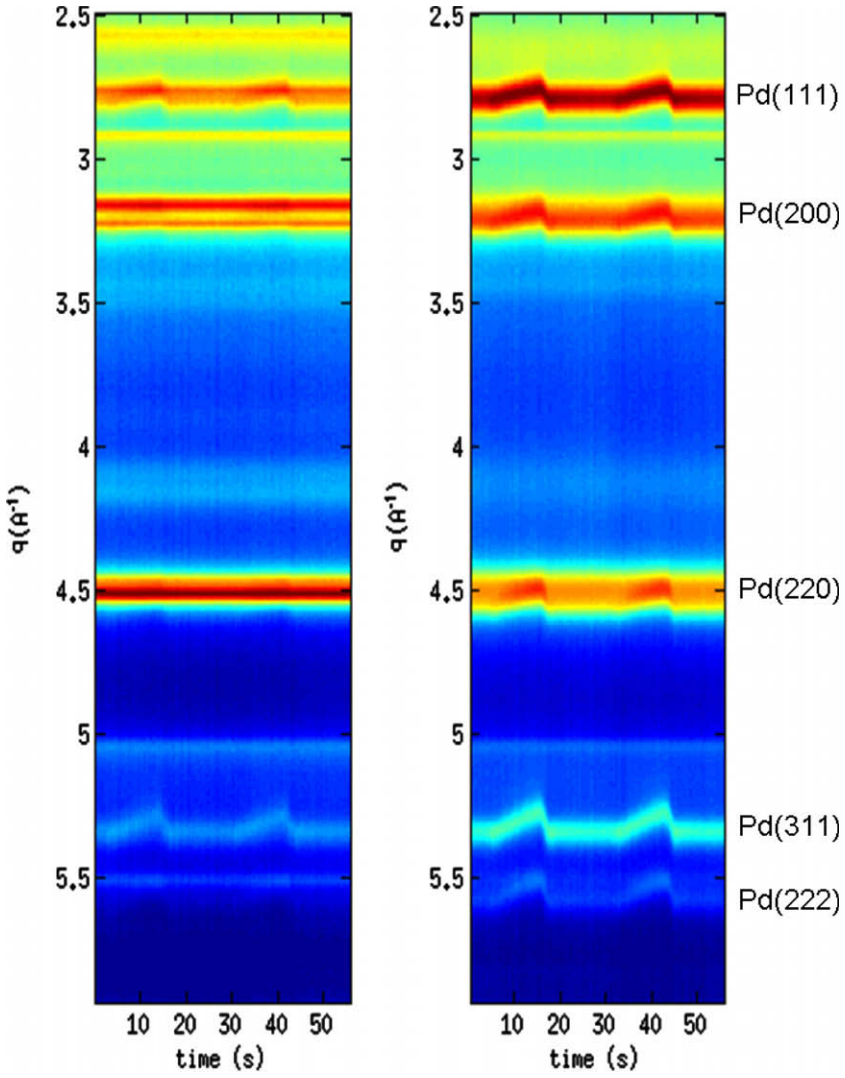

Fig. 3. XRD data over a CO/NO (5% in He; 75 ml min^{-1}) cycling treatment at 673 K (same temporal region as Fig. 1). Left 2PdA; right 4PdA. Samples are described as *x*PdA, where *x* is the noble metal weight loading percentage.

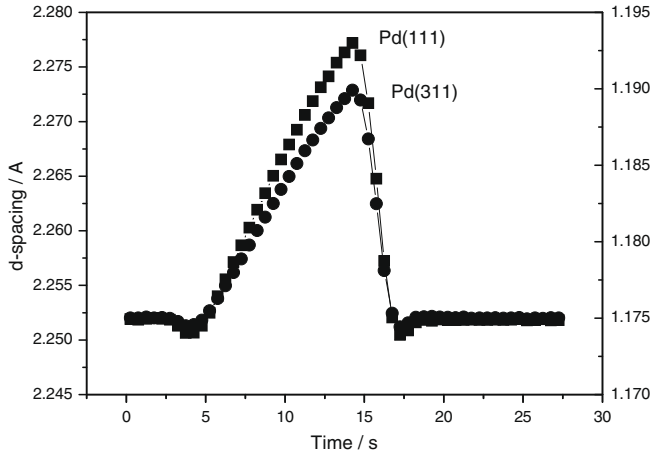

Fig. 4. XRD analysis of the Pd(1 1 1) (left OY scale) and Pd(3 1 1) (right OY scale) plane distance of the 4 wt.% Pd on alumina sample over a CO/NO (5% in He; 75 ml min^{-1}) cycling treatment at 673 K.

1PdA ≪ 2PdA ⩽ 4PdA with concomitant production of N_2 and CO_2. However, the normalized data describe another situation. Per Pd surface atom, relatively small differences are observed in CO and NO "surface" uptake (slightly higher for 1PdA and rather similar for the remaining samples) but more significant differences are observed in N_2 production and, particularly, for CO_2 production. While N_2 is mainly observed upon a NO atmosphere and is produced in the order 1PdA < 2PdA ≈ 4PdA, CO_2 production displays a similar trend to N_2 upon the NO atmosphere but appears in the order 1PdA > 2PdA > 4PdA in presence of CO gas.

4. Discussion

As deduced from our combined XAS/XRD structural study, Pd particles display a rather dynamic behaviour in response to changes in the atmosphere from reducing to oxidizing conditions. While here we only present a simplified view of the real phenomena that may occur, it is clear that the richness of the physicochemical phenomena occurring during our tested cycling conditions would take into account morphological as well as structural/phase changes of the noble metal particles. Concerning morphological modifications, shape changes have been previously observed for Pd and other noble metals like Rh, although these must be decoupled from oxidation effects produced upon the oxidizing step of the cycle [6,7,18,45]. In cases where this is done, and a fully metallic state is observed, as is the case here after the 3rd

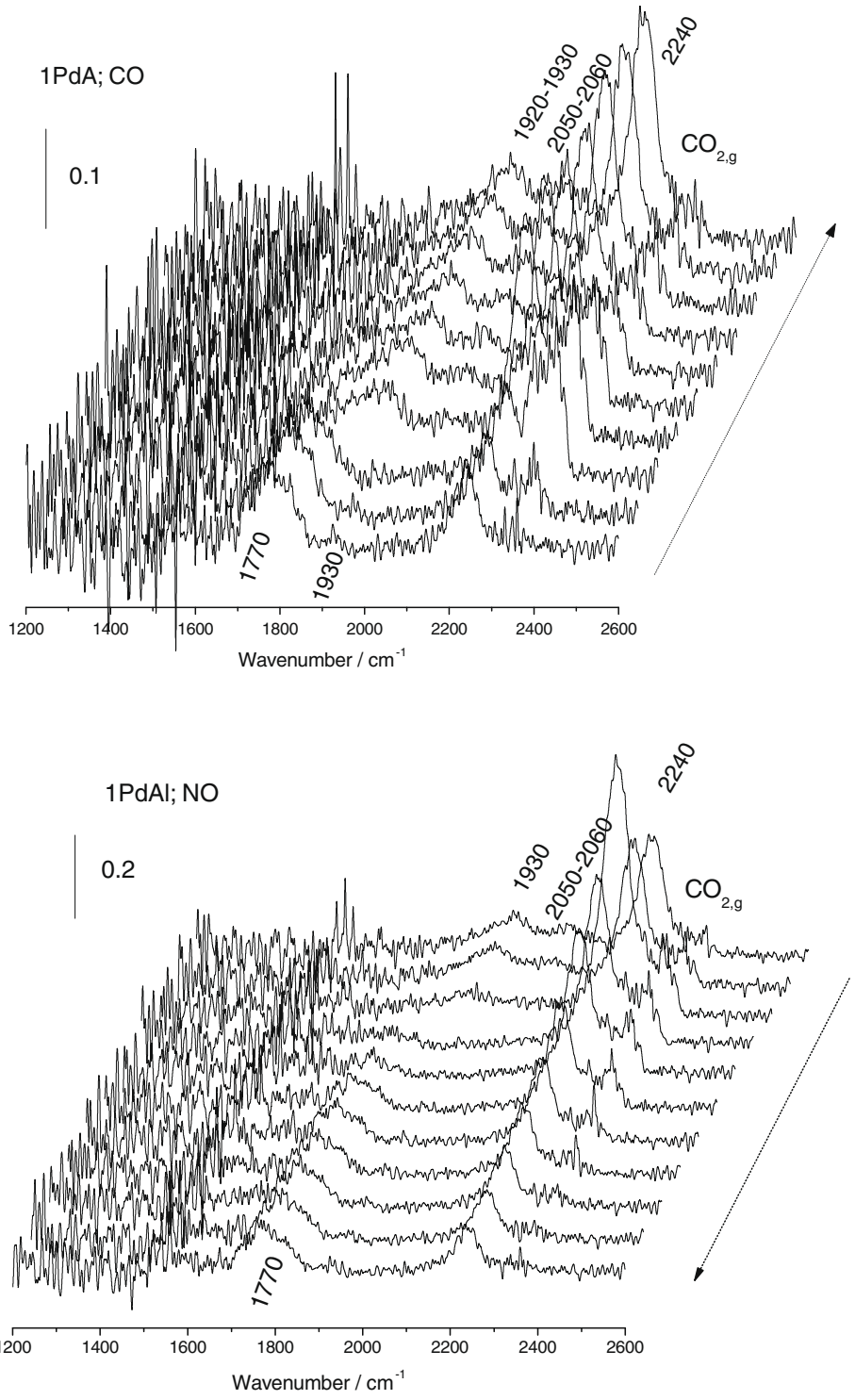

Fig. 5. IR data for the 1 wt.% Pd on alumina sample under a CO/NO (5% in He; 75 ml min^{-1}) cycling treatment at 673 K. Total temporal span (each plot): 13.84 s.

cycle, changes in Pd–Pd C.N.s can be ascribed to shape/size morphological modifications [6]. Size changes are demonstrated from the XRD study where a simple (Willianson–Hall) analysis of the peak width indicate size-effects. However, recent results also indicate the difficulty in decoupling size vs. strain within any current formalism (Willianson–Hall; Thomson–Cox–Hastings, etc.), providing evidence that a full study will be required to further progress in this direction [46].

A clear singularity in the results from the above-mentioned XRD/XAS analysis occurs for changes observed in the "valley" between maximum values of the C.N.s (Fig. 1); as proved by the XRD study (Figs. 3/4), there is the formation of a PdC_x phase which enhances static disorder among the metal nanoparticles and induces an erroneous estimation of the XAS C.N.s within the postulated (isothermal) constancy of the DW factor [33]. This fact has been taken into account in the dispersion plots presented in Fig. 1B. As similar maxima are obtained at the initial/final steps of the PdC_x existence, essentially no change in dispersion is estimated in such valley region of the Pd–Pd C.N.s. As presented in Fig. 1 and summarized in Table 1, we can observe that sample

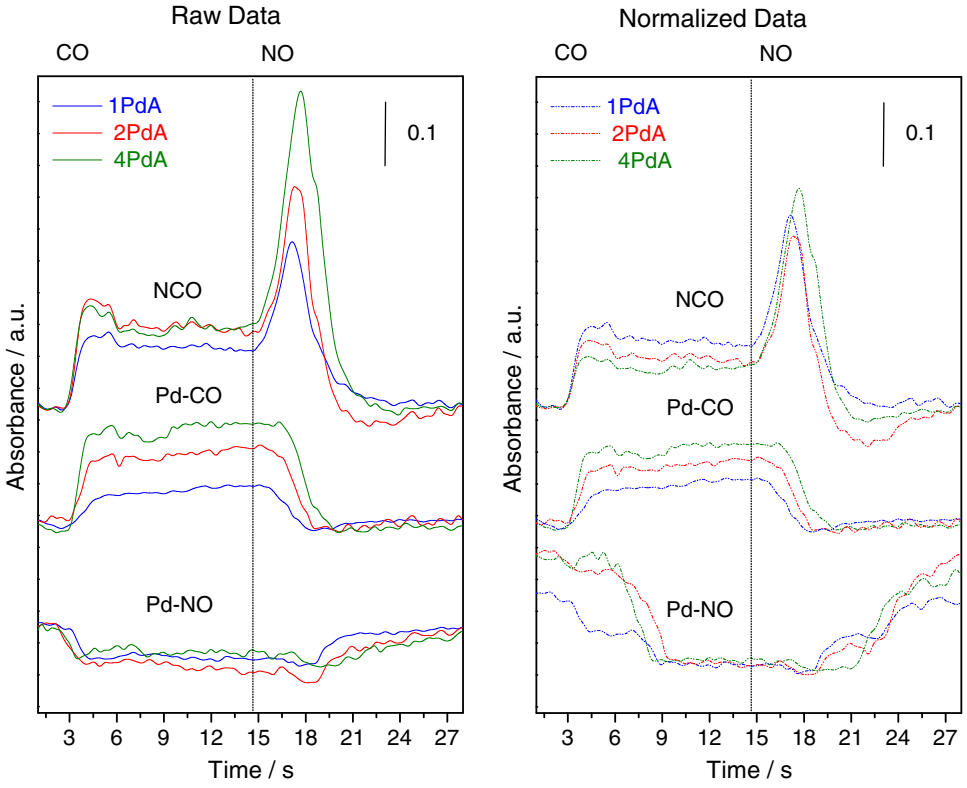

Fig. 6. IR intensity plot for the main adsorbate species observed for PdA samples during a CO/NO (5% in He; 75 ml min^{-1}) cycling treatment at 673 K. Raw and normalized (Pd atom surface basis) data are presented. The alumina NCO contribution (see Supporting Information file and text) is eliminated from the plot. Samples are described as *x*PdA, where *x* is the noble metal weight loading percentage.

1PdA goes from almost full dispersion to ca. 83% while 2Pd goes from ca. 82–57% and 4PdA from ca. 53–34%. There is a an important decrease in dispersion from 1PdA to 2PdA and a further decrease from 2PdA to 4PdA; the ratio between minimum and maximum dispersion values indicates that dispersion losses account for ca. 87%, 70%, and 63% of the initial dispersion for, respectively, 1PdA, 2PdA, and 4PdA samples. It is thus evident that, in relative terms, dispersion changes are at odds with a simple picture and increase as a function of the Pd loading or, in other words, as a function of the particle size. Fig. 9 provides in fact conclusive evidence of a rough linear dependence of the dispersion change upon the CO step and the inverse of the particle radius. Larger dispersion losses are therefore observed for larger particles which suffer stronger morphological phenomena. This inverse dependence is primarily governed by the particle radius.

Although the calculation of the dispersion is a semiquantitative result, which cannot fully decouple shape and size changes occurring in the metallic particles, it corresponds to a powerful tool in order to analyse chemical activity in terms of Pd surface atoms. Here, we can make a "dynamic" correction of DRIFTS and MS observables under operando, reaction conditions. In doing so, we attempt to interpret the physical phenomena occurring at the gas-phase interface in terms of the activity per active surface metal site. To simplify the discussion, in Table 1 we summarize the maximum and minimum values reached by the metal dispersion and the total available metal surface area for each sample. Total metal surface area values are relative and consider as unity the area of the 1PdA at its minimum. As comparison of Figs. 1 and 5/6 suggests, maximum values of both observables (e.g. metal dispersion and the total available metal surface area for each sample) are detected at the initial part of the CO step and essentially throughout all NO except when CO is present at the surface of the metal. Minimum values of dispersion are observed mainly throughout the CO step but more precisely while CO species are present at the surface. This correlation occurs for both raw and normalized data presented in Fig. 6 and clearly indicates the intimate relationship between the adsorbed surface entities and the morphological changes suffered by the metal particles. CO adsorption and/or dissociation (e.g. carbide formation) would be thus responsible for the initial growth of the Pd–Pd C.N. while the absence of such adsorbates at the surface reverses the process completely. As said, this appears a general phenomenon for all *x*PdA samples although it seems to be promoted with the parallel growth of the metal particle size (e.g. Table 1 the ratio between maximum and minim dispersion state grows with metal loading). So, as a first point, it appears that morphology changes upon dynamic, cycling conditions are size-dependent and favoured for higher particle sizes. Again, we note that Fig. 9 indicates that particle radius governs this morphology change in our set of analysed samples.

From a reactive perspective, the normalized DRIFTS and MS data allow to study the effect of the dynamic metal particle changes on the key reaction steps related, respectively, to adsorption and consumption of reactive molecules, CO and NO, and the production of N_2 and CO_2. Concerning adsorption of reactants, at the minimum dispersion stage, IR normalized metal surface coverage (e.g. NO) follows the trend 1PdA ≈ 2PdA ≈ 4PdA (Fig. 6) while the normalized NO gas-phase consumption (*M*/*z* 30 signal; Fig. 8B) appears as 1PdA ⩾ 2PdA ≈ 4PdA. It would thus appear that NO (molecular) adsorption is slightly favoured upon increase in Pd particle size, but with a rather mild trend for particle size above that of 2PdA [8,12,16]. In any case, a relatively weak size-dependence is detected by both techniques with more important consequences related to the NO ad-layer stability upon the CO step. At the maximum (e.g. largest Pd–Pd C.N.) dispersion stage, the

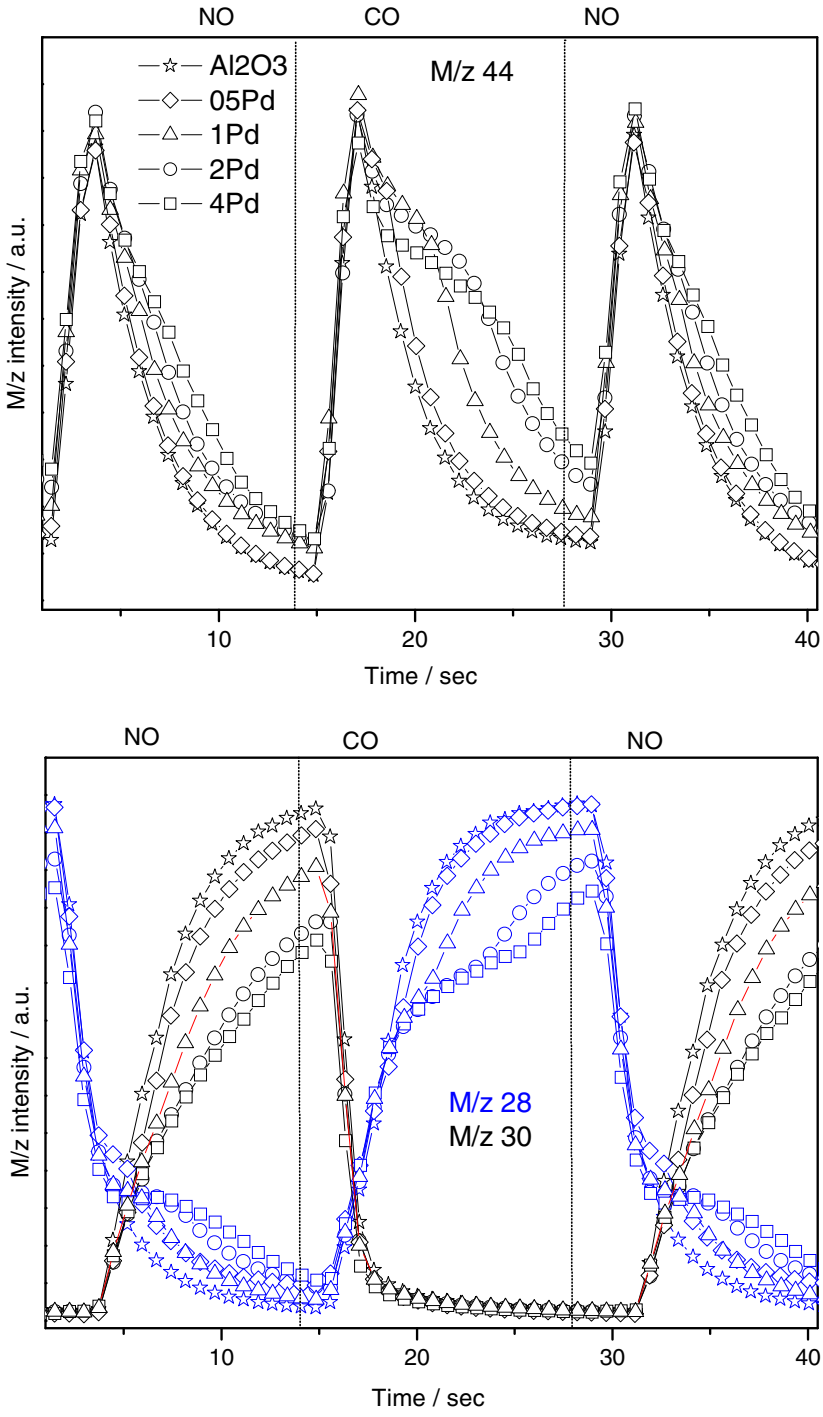

Fig. 7. MS results for selected M/z values under CO/NO (5% in He; 75 ml min^{-1}) cycling treatment at 673 K. Samples are described as xPdA, where x is the noble metal weight loading percentage.

normalized CO surface coverage as measured by DRIFTS evolves like 1PdA < 2PdA ⩽ 4PdA while consumption of gas-phase CO monitored by MS follows a slightly different trend (1PdA < 2PdA ≈ 4PdA; Fig. 8B). Both DRIFTS/MS normalized data show weak dependences with particle size if compared with corresponding raw data. We can thus deduce that intrinsic size-effects on adsorption steps upon reaction conditions are rather small and probably connected exclusively with NO. This is roughly in agreement with previous knowledge although a more drastic size-effect on NO may be envisaged [8,12,14,16,22]. The analysis allows to conclude that, concerning adsorption of reactants, differences between catalysts concerning raw DRIFTS/MS signals are primarily related with the total surface area available (Table 1) which explains the CO growing trend with particle size and the weaker apparent effect on NO adsorption.

The second point to discuss concerns the product formation pathways and their size sensitivity. As for N_2, we must discern between the two key steps involved; NO dissociation and N–N recombination. While NO dissociation might have kinetic significance in very small particles (like those of 1PdA), it is clear that the N–N recombination appears as the more likely reaction determining step. According to the literature, the facility of N–N

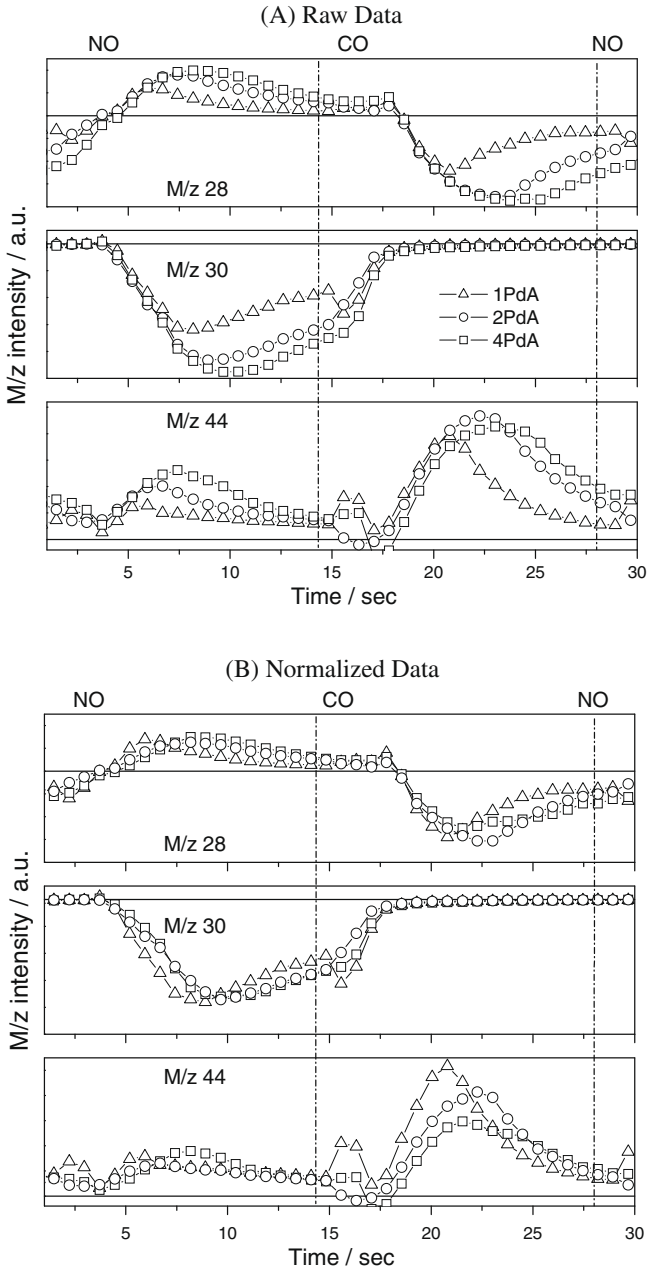

Fig. 8. MS difference (Al_2O_3 contribution subtracted) plots for PdA samples under CO/NO (5% in He; 75 ml min^{-1}) cycling treatment at 673 K. Raw and normalized (Pd surface atom basis) difference data are shown. Samples are described as *x*PdA, where *x* is the noble metal weight loading percentage.

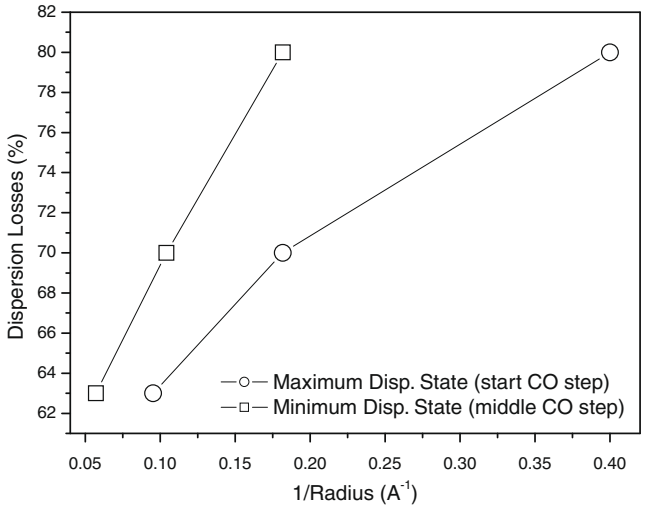

Fig. 9. Analysis of dispersion losses occurring during the CO step as a function of the inverse of the Pd particle radius.

coupling decreases as the Pd primary particle size is diminished [12,22,42,47]. Here, the formation of NCO in the presence of NO in the reactant atmosphere (Fig. 6) clearly indicates that NO dissociation per Pd surface atom is similar for all samples, with the absence of significant differences between all studied samples. So, the differences in N_2 formation (normalized MS signal in Fig. 8B; upper panel) seem to follow a weak trend 1PdA < 2PdA ≈ 4PdA, in relative agreement with the expected size-dependence of the N–N coupling step. In our case, the size-sensitivity appears to be lost or strongly diminished for sizes above 2PdA.

In the case of CO_2, we can distinguish between the production in presence of adsorbed CO or NO as major species at metal species. In the NO atmosphere part of the cycle, CO_2 production is relatively limited and only observed where the majority of CO is eliminated from the surface. In spite that in this part of the cycle N_2 and CO_2 appear concomitantly generated (Fig. 8B), CO_2 production apparently lacks clear size-sensitivity. This would agree with the common view that CO desorption is the limiting step for CO_2 formation, although, as mentioned, a weak size-dependence is expected for this elemental reaction step [17,22]. A slightly higher normalized MS signal is observed for 4PdA and may be related to a larger presence of oxygen ad-species at the surface. However, as no clear differences can be deduced on NO dissociation from NCO (DRIFTS data upon a NO atmosphere), the later point would likely indicate differences in Pd–O interaction.

CO_2 evolves to the gas phase mainly upon the CO part of the cycle and follows the trend 1PdA > 2PdA > 4PdA (bottom panel in Fig. 8B normalized MS signal). As Fig. 6 indicates a normalized CO surface coverage with a mild size dependence with a contrasting behaviour with respect to MS signal, this would indicate that CO_2 production is dominated (again) by the desorption of the CO molecule and the availability of surface free sites with oxygen-containing fragments in the neighbourhood. The size-dependence of the CO desorption step has been previously postulated [17,22], and potential alternatives to rationalize this behaviour in terms of the oxygen supply seem hardly acceptable as we did not detect any PdO_x formation by XANES (bulk species) or by DRIFTS (e.g. formation of partially oxidized palladium surface species at the surface of the materials as probed by adsorbate, e.g. CO, characteristics). Figs. 3/4, however, indicate another alternative could be CO_2 produced from the Boudouard reaction on a stoichiometric basis with storage the C fragments within the Pd nanoparticles detected by XRD and in EXAFS [33]. Comparison with known carbon storage capability (PdC_x with $x = 0.065$, 0.095, and 0.08 for, respectively, 1PdA, 2PdA, and 4PdA) shows the absence of correlation and, therefore, the small involvement of PdC_x species in CO_2 formation. The main point to stress is thus the observed size-sensitivity for CO_2 formation upon the reducing part of the cycle, which could be ascribed to the CO desorption step.

As a final point, we may comment a few words on NCO formation. Upon a NO atmosphere, this molecule is formed from dissociated CO in the reducing part of the cycle and, curiously, from non-dissociated NO in the oxidizing part. As previously mentioned, upon decomposition in a NO atmosphere, the PdC_x may not evolve giving CO_2 and thus is majorly eliminated *via* NCO formation. This molecule is thus formed by several paths involving a $NO + CO \rightarrow NCO + O_a$ step upon all conditions and the $CO + N_a \rightarrow NCO$ and $NO + PdC_x \rightarrow NCO + Pd$ steps at, respectively, the reducing and

oxidizing parts of the cycle. The importance of the new NO and PdC_x pathway formation where un-dissociated NO is activated and forms NCO may reside in presence of hydrocarbons as the carbon supply to the Pd nanoparticles would be significantly favoured. As a result, this route to the NCO species would become intrinsically more likely and would permit these intermediates to be populace enough to significantly affect the activity/selectivity of de-NO_x processes upon cycling, lambda oscillations [48,49].

5. Conclusions

The study presents a synchronous XAS, DRIFTS and MS study attempting to analyse the dynamic behaviour of the Pd/Al_2O_3 system upon CO/NO cycling conditions. Pd morphology changes were examined with EXAFS and a general, reversible phenomenon is observed upon cycling conditions. This happens in the whole Pd size region scanned (e.g. dispersion from 1 to 0.4) and, contrarily to simple expectations, larger dispersion variations are observed for larger particles, which suffer stronger morphological modification.

With the help of the C.N. obtained from EXAFS, we analysed the chemical response of three PdA samples to the gas cycling conditions and tried to establish the Pd size-dependence of all relevant chemical step concerning reactant gas adsorption, dissociation, and activation steps. It was founded that potential size-dependences display significant differences with respect to expected results based on non-cycling measurements, typically performed with a fixed (most times stoichiometric) gas atmosphere. Particularly, most interesting results concern, in first place, to the absence of a marked size-sensitivity for all relevant N_2 formation steps. This takes into account both the NO dissociation step but particularly the N–N coupling. The study showed that differences among samples in N_2 formation are mostly justified by the metal surface area available and that the presumed size-sensitivity of the two elemental steps does not influence N_2 formation. CO_2 formation seems, on the other hand, dominated by the CO desorption step and, contrarily to prototypical assumptions originated from measurements at non-cycling conditions, may present an important size-dependence. The growth of the Pd particle size was thus founded detrimental for production of CO_2. The structure–activity relationship for Pd particles in CO and NO elimination reactions would thus display a characteristic size-dependence upon dynamic conditions, far from that predicted by non-cycling measurements.

In addition to this, the study was able to show a novel route for NCO formation taking place from un-dissociated NO and C fragments present at the metal phase and coming from dissociated CO. The importance of this finding may be enhanced in presence of hydrocarbons and may lead to new routes for CO activation.

Acknowledgments

The authors would like to thank the ESRF for access to facilities and for the funding that has permitted the development of this experiment on ID24. Trevor Mairs, Pascale Dideron, Dominique Rohlion, and Marchial Lambert are gratefully thanked for their extensive technical contributions to the modifications of the DRIFTS optics required to make this experiment fully compatible with the HXRD experiment. Dr. Viejo Honkimaki is also thanked for his general support and stewardship of ID15. Finally, we acknowledge the CYCIT–Spain (CTQ2007-060480/BQU) for financial support. A.K. thanks CSIC for a I3P postdoctoral Grant.

Appendix A. Supplementary data

Supplementary data associated with this article can be found, in the online version, at doi:10.1016/j.jcat.2010.01.008.

References

[1] H.F. Rose, Handbook of commercial Catalysts, CRC Press, Boca Raton, 2000.
[2] E.S.J. Lox, B.H. Engler, in: G. Ertl, H. Knözinger, H.J. Weitkamp (Eds.), Environmental Catalysis, Wiley-VCH, 1999, p. 1.
[3] A. Martínez-Arias, J.C. Conesa, M. Fernández-García, J.A. Anderson, in: J.A. Anderson, M. Fernández-García (Eds.), Supported Metals in Catalysis, Imperial College Press, Singapore, 2005, p. 283.
[4] J. Kašpar, P. Fornasiero, in: A. Trovarelli (Ed.), Catalysis by Ceria and Related Materials, Imperial College Press, Singapore, 2002, pp. 224–228 (Chapter 6).
[5] J.R. González-Velasco, J.A. Botas, R. Farret, M.P. González-Marcos, J.L. Marc, M.A. Gutierrez-Ortiz, Catal. Today 59 (2000) 395.
[6] M.A. Newton, C. Belver-Coldeira, A. Martínez-Arias, M. Fernández-García, Nat. Mater. 6 (2007) 528.
[7] M.A. Newton, C. Belver-Coldeira, A. Martínez-Arias, M. Fernández-García, Angew. Chem. Int. Ed. 46 (2007) 8629.
[8] A. Iglesias-Juez, A. Martínez-Arias, M. Fernández-García, J. Catal. 221 (2004) 148.
[9] X. Wu, D. Weng, Appl. Surf. Sci. 221 (2004) 375.
[10] A. Iglesias-Juez, A. Martínez-Arias, M.A. Newton, S.G. Fiddy, M. Fernández-García, Chem. Commun. (2005) 4092.
[11] T. Yammamoto, A. Suzuki, Y. Nagai, T. Tanabe, F. Dong, Y. Inada, M. Nomura, Y. Iwasawa, Angew. Chem. Int. Ed. 46 (2007) 9253.
[12] A. Martínez-Arias, A.B. Hungría, M. Fernández-García, A. Iglesias-Juez, J.A. Anderson, J.C. Conesa, J. Catal. 221 (2004) 85.
[13] M.Q. Shen, M. Yang, J. Wang, J. Wen, M. Zhao, W.L. Wang, J. Phys. Chem. C 113 (2009) 3212.
[14] M. Yang, M. Shen, J. Wang, J. Wen, M. Zhao, W. Wang, J. Phys. Chem. C 113 (2009) 12778.
[15] X. Xu, D.W. Goodman, J. Phys. Chem. 97 (1993) 7711.
[16] D.R. Rainier, M. Koranne, S.M. Vesecky, D.W. Goodman, J. Phys. Chem. B 101 (1997) 10769.
[17] J. Hoffmann, I. Meusel, J. Hatmann, J. Libuda, H.-J. Freund, J. Catal. 204 (2001) 378.
[18] B. Huber, P. Koskinene, H. Hakkinen, M. Moseler, Nat. Mater. 5 (2006) 44.
[19] T. Schallow, B. Brandt, D.E. Starr, M. Laurin, S.K. Shaikhutdinov, S. Schauermann, J. Libuda, H.-J. Freund, Phys. Chem. Chem. Phys. 9 (2007) 1347.
[20] A. Wille, P. Nickut, K. Al-Shamery, J. Mol. Struct. 695–696 (2004) 345.
[21] J.H. Holles, R.J. Davis, Th.M. Murray, J.M. Howe, J. Catal. 195 (2000) 193.
[22] J. Libuda, H.-J. Freund, Surf. Sci. Rep. 57 (2005) 157.
[23] G. Agostini, R. Pellegrini, G. Leofanti, L. Birtinetti, S. Bertarione, E. Groppo, A. Zecchina, C. Lamberti, J. Phys. Chem. C 113 (2009) 10485.
[24] A.M. Beale, Ad.M.J. van der Eerden, K. Kervinen, M.A. Newton, B.M. Weckhuysen, Chem. Commun. (2005) 3015.
[25] A.M. Beale, Ad.M.J. van der Eerden, S.D.M. Jacques, O. Leynaud, M.G. O'Brien, F. Meneau, S. Nikitenko, W. Bras, B.M. Weckhuysen, J. Am. Chem. Soc. 128 (2006) 12386.
[26] B.M. Weckhuysen, Angew. Chem. Int. Ed. 48 (2009) 4910.
[27] M.A. Newton, Top. Catal. 52 (2009) 1410.
[28] M. Fernández-García, A. Iglesias-Juez, A. Martínez-Arias, A.B. Hungría, J.A. Anderson, J.C. Conesa, J. Soria, Appl. Catal. B 31 (2001) 39.
[29] M.A. Newton, J. Synchrotron Radiat. 14 (2007) 372.
[30] J.-C. Labiche, O. Mathon, S. Pascarelli, M.A. Newton, G. Guilera Ferre, C. Curfs, G. Vaughan, A. Homs, D. Fernandez Carreiras, Rev. Sci. Instrum. 78 (2007) 091301.
[31] A. Jentys, Phys. Chem. Chem. Phys. 1 (1999) 4059.
[32] C De Boor, A Practical Guide to Splines, Springer-Verlag, NY, 1978.
[33] M.A. Newton, M. Di Michiel, A. Kubacka, M. Fernández-García, submitted for publication.
[34] J.A. McCaulley, Phys. Rev. B 47 (1993) 4872.
[35] J.A. McCaulley, J. Phys. Chem. 97 (1993) 10372.
[36] M. Maciejewcki, A. Baiker, J. Phys. Chem. 98 (1994) 285.
[37] F. Viñes, C. Loschen, F. Illas, K.M. Neyman, J. Catal. 266 (2009) 59.
[38] F. Illas, N. López, J.M. Ricart, A. Clotet, J.C. Conesa, M. Fernández-García, J. Phys. Chem. B 102 (1998) 8017.
[39] E. Ozensoy, C. Hess, D.W. Goodman, Top. Catal. 28 (2004) 13.
[40] R. Nemeth, J. Kiss, F. Solymosi, J. Phys. Chem. B 111 (2007) 1424.
[41] P. Hollins, Surf. Sci. Rep. 16 (1992) 51.
[42] M. Fernández-García, A. Martínez-Arias, N.L. Salamanca, J.M. Coronado, J.A. Anderson, J.C. Conesa, J. Soria, J. Catal. 187 (1999) 474.
[43] J. Changho, T. Hideyucki, K. Michisima, K. Momoji, B. Ewa, M. Akira, Catal. Today 111 (2006) 322.
[44] M.A. Vannice, C.C. Twu, J. Phys. Chem. 75 (1981) 5944.
[45] P. Nolte, A. Stierle, N.Y. Jin-Phillipp, N. Kasper, T.U. Schulli, H. Dosch, Science 321 (2008) 1654.
[46] S. Vives, C. Meunier, Powder Diffract. 24 (2009) 205.
[47] A.S. Worz, K. Juday, S. Abbeh, O. Heiz, J. Am. Chem. Soc. 125 (2003) 7964.
[48] N. McCleod, R.M. Lambert, Appl. Catal. B 46 (2003) 483.
[49] N. McCleod, R.M. Lambert, Chem. Commun. (2003) 1300.